Hindawi
Advances in Civil Engineering
Volume 2019, Article ID 4627174, 8 pages
https://doi.org/10.1155/2019/4627174

Research Article

Application of a Viscoelastic Model to Creep Settlement of High-Fill Embankments

Liang Jia and Guangli Huang

College of Civil Engineering, Lanzhou University of Technology, Lanzhou 730050, China

Correspondence should be addressed to Guangli Huang; hgl19957@163.com

Received 30 January 2019; Revised 2 June 2019; Accepted 25 June 2019; Published 28 July 2019

Academic Editor: Hui Yao

In order to predict the creep settlement of high-fill embankments, the time-dependent viscoelastic model of Poynting–Thomson (the standard linear solid) has been chosen to represent the creep behavior of soils. In the present study, the hereditary integral was applied to calculate the strain while the load increase is varied with time. Calculation expressions of the creep settlement of an embankment during and after construction were obtained under one-dimensional compression conditions. Using this approach, the three parameters of every layer can be determined and adjusted to accommodate in situ monitoring data. The calculated results agreed well with those from the field, which imply that the method proposed in this paper can give a precise prediction of creep settlement of high-fill embankments.

1. Introduction

Creep settlement is a main research issue for highway deterioration and other high-fill projects [1–5]. The analysis of embankment creep settlements is the basis for the correct understanding and evaluation of the subgrade stability. In consequence, more research should be carried out into the calculation of creep settlement of embankment. Existing methods related to creep settlement research can be divided into three groups: (1) Empirical models, for example, the Asaoka method [6, 7], the hyperbolic method [8], the parabola method [9], the exponential method, and in situ tests [10, 11], in those methods, the monitored creep settlement of the embankment after construction was adopted to predict the creep settlement in the future. (2) Constitutive models: Bjerrum [12] pointed out that the influence of creep on clays was equivalent to make the clay overconsolidated, which was obtained through a large number of consolidation tests and engineering settlement data analysis, and Yao et al. [13] established the unified hardening (UH) model (a model for over-consolidated clays), which considered the time effects and analyzed the influence of creep on over-consolidated clays. Hashiguchi [14] put forward the concept of a subloading yield surface. Asaoka et al. [15] suggested the concept of superloading and subloading yield surfaces for over-consolidated soils. And Wang et al. [16] proposed an advanced elastic-viscoplastic constitutive model to predict time-dependent behavior of the over-consolidated clay based on the subloading surface model and relative overstress relation. (3) Numerical methods: Loganathan et al. [17] put forward a calculation method named "field deformation analysis" (FDA), which separates and quantifies settlement components. Li et al. [18] used the modified secant modulus method to calculate settlements, an approach that is characterized by the fact that it is not influenced by the initial void ratio. But the empirical models pay less attention on the creep mechanism of clays, and most of the constitutive models are elastoplastic constitutive models, which cannot describe the time-dependent deformation characteristic of over-consolidated clays. Experimental results indicate that the creep deformation of high-filled embankment is affected by both time and stress history. The rheological model can reflect the time-dependent stress-strain behavior of clays, and in order to simulate the layered filling process of the high-filled embankment during construction, the stress applied on the rheological model is

according to the loading curve, so the rheological model used in the creep settlement calculation of the embankment can not only reflect the time-dependent stress-strain behavior but also the stress history of the embankment. The application of some relatively simple rheological models has been studied in some cases [19–22]. Morro [23] concluded that a spring-dashpot model (i.e., the Maxwell model in parallel with a dashpot) showed a constant strain rate during the secondary stage. Justo and Durand [24] obtained settlement expressions with the standard linear solid rheological model for one-dimensional settlements of an embankment during and after construction. In this paper, the Poynting–Thomson model (a linear spring in parallel with a Maxwell model) was applied to represent the time-dependent deformation of soil, and the theory of the hereditary integral used to calculate the cumulative strain is explained in detail, which reflects the strain at any time factor T and depends upon the entire stress history [25, 26].

As an illustration of the creep settlement performance of a high-filled embankment, the case of the dam-like embankment of the Lanzhou–Yongjing highway was investigated using the proposed new method.

2. Theory

For the model of Poynting–Thomson (Figure 1),

$$\sigma = \sigma_{\mathrm{M}} + \sigma_{\mathrm{H}}, \tag{1}$$

$$\varepsilon = \varepsilon_{\mathrm{M}} = \varepsilon_{\mathrm{H}}, \tag{2}$$

where

$$\sigma_{\mathrm{H}} = E_{\mathrm{H}}\varepsilon_{\mathrm{H}} = E_{\mathrm{H}}\varepsilon. \tag{3}$$

The constitutive equation of the Maxwell model in Figure 1 is

$$\frac{\eta}{E_{\mathrm{M}}}\dot{\sigma_{\mathrm{M}}} + \sigma_{\mathrm{M}} = \eta\dot{\varepsilon_{\mathrm{M}}}, \tag{4}$$

where

$$\dot{\sigma_{\mathrm{M}}} = \dot{\sigma} - \dot{\sigma_{\mathrm{H}}}, \tag{5}$$

$$\dot{\varepsilon_{\mathrm{M}}} = \dot{\varepsilon}. \tag{6}$$

Substituting equations (5) and (6) into equation (4) yields

$$\frac{\eta}{E_{\mathrm{M}}}\left(\dot{\sigma} - \dot{\sigma_{\mathrm{H}}}\right) + \sigma_{\mathrm{M}} = \eta\dot{\varepsilon_{\mathrm{M}}}. \tag{7}$$

The calculation expression of σ_{M} is obtained from equation (7):

$$\sigma_{\mathrm{M}} = \eta\dot{\varepsilon_{\mathrm{M}}} - \frac{\eta}{E_{\mathrm{M}}}\left(\dot{\sigma} - \dot{\sigma_{\mathrm{H}}}\right), \tag{8}$$

and substituting the expressions of σ_{M} and equation (3) into equation (1) yields

$$\sigma - E_{\mathrm{H}}\varepsilon = \eta\dot{\varepsilon} - \frac{\eta}{E_{\mathrm{M}}}\left(\dot{\sigma} - \dot{\sigma_{\mathrm{H}}}\right) = \eta\dot{\varepsilon} - \frac{\eta}{E_{\mathrm{M}}}\left(\dot{\sigma} - E_{\mathrm{H}}\dot{\varepsilon}\right). \tag{9}$$

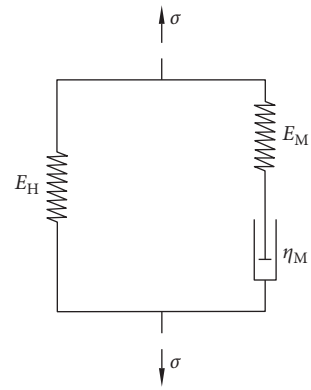

Figure 1: Viscoelastic model.

The constitutive equation of the Poynting–Thomson model is

$$\frac{\eta}{E_{\mathrm{M}}}\dot{\sigma} + \sigma = \frac{\eta}{E_{\mathrm{M}}}\left(E_{\mathrm{M}} + E_{\mathrm{H}}\right)\dot{\varepsilon} + E_{\mathrm{H}}\varepsilon. \tag{10}$$

In a creep test, the pressure maintains a constant value σ_0 when $t = 0$; equation (10) becomes

$$\sigma = \frac{\eta}{E_{\mathrm{M}}}\left(E_{\mathrm{M}} + E_{\mathrm{H}}\right)\dot{\varepsilon} + E_{\mathrm{H}}\varepsilon. \tag{11}$$

The Poynting–Thomson model (Figure 1) first produces the instantaneous elastic deformation $\varepsilon_0 = \sigma_0/(E_{\mathrm{M}} + E_{\mathrm{H}})$ under the constant pressure σ_0. As time increases, the deformation continues to increase such that when $t \longrightarrow \infty$, $\varepsilon \longrightarrow \sigma_0/E_{\mathrm{M}}$, and the solution of equation (11) is

$$\varepsilon(T) = \frac{\sigma_0}{E_{\mathrm{H}}}\left[1 - \frac{E_{\mathrm{M}}}{E_{\mathrm{M}} + E_{\mathrm{H}}}e^{-\left(\left(E_{\mathrm{M}}E_{\mathrm{H}}\right)/\left(E_{\mathrm{M}}+E_{\mathrm{H}}\right)\eta\right)t}\right]. \tag{12}$$

Which otherwise can be written as

$$\varepsilon(t) = \frac{\sigma_0}{E_{\mathrm{H}}}\left[1 - Re^{-T}\right], \tag{13}$$

where

$$R = \frac{E_{\mathrm{M}}}{E_{\mathrm{M}} + E_{\mathrm{H}}}. \tag{14}$$

R is called the creep factor.

$$T_{\mathrm{r}} = \frac{E_{\mathrm{M}}E_{\mathrm{H}}}{\left(E_{\mathrm{M}} + E_{\mathrm{H}}\right)\eta}. \tag{15}$$

$T = t/T_{\mathrm{r}}$ is called the time factor.

And equation (13) can also be written as

$$\varepsilon(t) = \sigma_0 J(T), \tag{16}$$

where

$$J(T) = \frac{1}{E_{\mathrm{H}}}\left[1 - Re^{-T}\right]. \tag{17}$$

The mechanical meaning of $J(T)$ is the strain under unit force, which can easily be measured in practical tests. $J(T)$ is called the creep compliance. After applying the stress σ_0 when $T = 0$, the strain of the model is $\sigma_0 J(T)$. Then, when

another stress $\Delta\sigma'$ is applied when $T = T'$, there is another strain $\Delta\sigma' J(T - T')$, which is added to $\sigma_0 J(T)$ when $T = T'$, which is proportional to $\Delta\sigma'$. This strain is also a function of T, but only adds $\varepsilon(t)$ when $T = T'$ and is still dependent upon the same creep compliance:

$$\varepsilon(T) = \sigma_0 J(T) + \Delta\sigma' J(T - T'). \tag{18}$$

If $\Delta\sigma''$ is applied when $T = T''$, then $\varepsilon(T)$ should increase $\Delta\sigma'' J(T - T'')$. The effect of each $\Delta\sigma$ on $\varepsilon(T)$ can be superposed in this way, which is called the Boltzmann superposition principle [27]. If σ changes when $T = 0$, the relationship between applied stress and the time factor T will be replaced by a stepped polyline, as shown in Figure 2. When $dT' \longrightarrow 0$, the sum becomes integral:

$$\varepsilon(T) = \int_0^T J(T - T') d\sigma(T'). \tag{19}$$

If the applied load varies with time, according to Figure 3, because $\sigma_0 = 0$, the strain at time factor T will be given by the hereditary integral:

$$\varepsilon(T) = \int_0^T \frac{1}{E_H}\left[1 - Re^{-(T-T')}\right]\frac{d\sigma}{dT'} dT'. \tag{20}$$

The solution of the hereditary integral is

$$\varepsilon(T) = \frac{1}{E_H}\left[\sigma - Re^{-T} I_1\right], \tag{21}$$

where

$$I_1(\sigma, T) = \int_0^T e^{T'} \frac{d\sigma}{dT'} dT'. \tag{22}$$

The strain from T to T_c (Figure 3) can be described as

$$\Delta\varepsilon(T, T_c) = \varepsilon(T_c) - \varepsilon(T)\,(T \le T_c). \tag{23}$$

$\Delta\varepsilon(T, T_c)$ is obtained from equation (21):

$$\Delta\varepsilon(T, T_c) = \frac{1}{E_H}\left[(\sigma_c - \sigma) - R\left(e^{-T_c} I_1(\sigma, T_c) - e^{-T} I_1(\sigma, T)\right)\right]. \tag{24}$$

And when $T \ge T_c$, the strain from T_c to T is (Figure 3)

$$\Delta\varepsilon(T_c, T) = \varepsilon(T_c) - \varepsilon(T). \tag{25}$$

From equation (21), it is supposed that the stress maintains a constant value when $T \ge T_c$ (Figure 3):

$$\Delta\varepsilon(T_c, T) = \varepsilon(T_c + DT) - \varepsilon(T_c) = \frac{R}{E_H} e^{-T_c} I_1(\sigma, T_c)\left(1 - e^{-DT}\right). \tag{26}$$

3. Application to a High-Filled Embankment

If it is assumed that the height of an embankment varies with time according to Figure 4, the stress at any point depends on the height of fill above it.

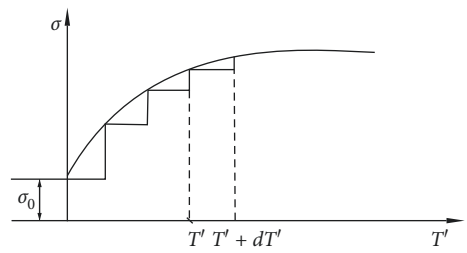

Figure 2: Sketch of the loading curve.

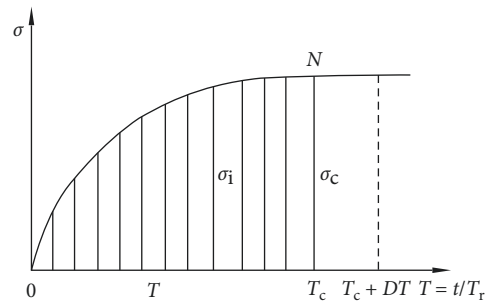

Figure 3: Variation of loading with time.

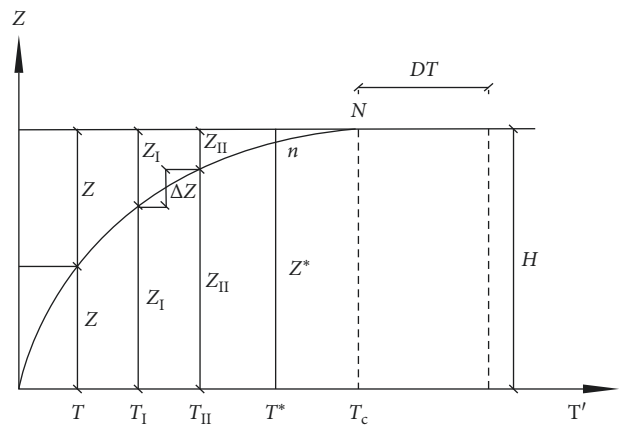

Figure 4: Variation of fill height with time.

3.1. Settlement of the Embankment during Construction

3.1.1. Degree of Settlement of the Embankment at Height z_I during Construction. The degree of settlement of the embankment at height z_I during construction can be described as follows:

$$S(z_I) = \int_0^{z_I} \Delta\varepsilon(T_I - T, T_c - T) dz. \tag{27}$$

$\Delta\varepsilon$ can be obtained from equation (21):

$$\frac{\Delta\varepsilon E_H}{\gamma} = Z_I - R\Big(e^{-T_c}\left[I_1(z, T_c) - I_1(z, T_I)\right] - e^{-T_I}\left[I_1(z, T_I) - I_1(z, T)\right]\Big), \tag{28}$$

where

$$I_1(z,T_I)=\int_0^{T_I}e^{T'}\frac{dz}{dT'}dT', \tag{29}$$

$$\begin{aligned}I_1(z,T_c)&=\int_0^{T_c}e^{T'}\frac{dz}{dT'}dT'=\int_0^{T_I}e^{T'}\frac{dz}{dT'}dT'\\&\quad+\int_{T_I}^{T_c}e^{T'}\frac{dz}{dT'}dT'.\end{aligned} \tag{30}$$

The integrals listed above must be calculated by numerical methods. In order to do this, the loading curve is divided into N intervals; from $T=0$ up to $T=T_I$, the curve is divided into I intervals, and from $T=T_I$ up to $T=T_c$, the curve is divided into $N-I$ intervals.

Substituting equation (28) into equation (27), the settlement of a point at height z_I during construction is obtained from

$$\frac{S(z_I)E_H}{\gamma}=Z_Iz_I-R\left[a-e^{-T_I}I_2(z,T_I)\right], \tag{31}$$

where

$$a=e^{-T_c}\left[z_II_1(T_I,T_c)+I_2(z,T_I)\right], \tag{32}$$

$$I_1(T_I,T_c)=\int_{T_I}^{T_c}e^T\frac{dz}{dT}dT=\sum_{i=I}^{N}\left(e^{T_i}\Delta z_i\right), \tag{33}$$

$$\begin{aligned}z_i&=\frac{z_{I+1}-z_{I-1}}{2},\\z_{I-1}&=z_I,\\z_{N+1}&=z_N,\end{aligned} \tag{34}$$

$$\begin{aligned}I_2(z,T_I)&=\int_0^{T_I}ze^T\frac{dz}{dT}dT=\sum_{i=1}^{I}\left(z_ie^{T_i}\Delta z_i\right),\\z_{I+1}&=z_N.\end{aligned} \tag{35}$$

If it is assumed that the height of the embankment increases linearly with time, and in order to simplify the deduction process, we assumed that the slope of the loading curve is 1, and then equations (33) and (35) will become

$$I_1(T_I,T_c)=\int_{T_I}^{T_c}e^T\frac{dz}{dT}dT=\int_{T_I}^{T_c}e^TdT=e^{T_c}-e^{T_I}, \tag{36}$$

$$I_2(z,T_I)=\int_0^{T_I}ze^T\frac{dz}{dT}dT=\int_0^{T_I}Te^TdT=T_Ie^{T_I}-e^{T_I}+1. \tag{37}$$

Substituting equations (36) and (37) into equation (31) gives

$$\frac{S(z_I)E_H}{\gamma}=Z_Iz_I-R\left(1+e^{-H}-e^{-Z_I}-e^{-z_I}\right). \tag{38}$$

3.1.2. Settlement of a Finite Layer (z_I,z_{II}) during Construction. The strain from time factor T_{II} up to T_c is

$$\Delta\varepsilon=\Delta\varepsilon(T_{II}-T,T_c-T). \tag{39}$$

Substituting T_I by T_{II} and equation (39) into equation (21) gives

$$\begin{aligned}\frac{\Delta\varepsilon E_H}{\gamma}&=(H-z_{II})-R\Big(e^{-T_c}\left[I_1(z,T_c)-I_1(z,T)\right]\\&\quad-e^{-T_{II}}\left[I_1(z,T_{II})-I_1(z,T)\right]\Big).\end{aligned} \tag{40}$$

The compression of a finite layer is

$$S(z_I,z_{II})=\int_{z_I}^{z_{II}}\Delta\varepsilon dz. \tag{41}$$

Substituting equation (40) into equation (41) gives

$$\begin{aligned}\frac{S(z_I,z_{II})E_H}{\gamma}&=(H-z_{II})\Delta z-R\Big[e^{-T_c}\Delta zI_1(T_{II},T_c)\\&\quad+b\Delta z\left(e^{-T_c}-e^{-T_{II}}\right)\Big],\end{aligned} \tag{42}$$

where

$$\Delta z=z_{II}-z_I, \tag{43}$$

$$b=\frac{I_2(T_I,T_{II})-z_II_1(T_I,T_{II})}{\Delta z}, \tag{44}$$

$$I_2(T_I,T_{II})=\int_{T_I}^{T_{II}}ze^T\frac{dz}{dT}dT=\sum_{i=I}^{i=II}\left(z_ie^{T_i}\Delta z_i\right), \tag{45}$$

$$I_1(T_I,T_{II})=\int_{T_I}^{T_{II}}e^T\frac{dz}{dT}dT=\sum_{i=I}^{i=II}\left(e^{T_i}\Delta z_i\right), \tag{46}$$

$$\begin{aligned}\Delta z_i&=\frac{z_{i+1}-z_{i-1}}{2},\\z_{II+1}&=z_{II},\\z_{II+1}&=z_{II}.\end{aligned} \tag{47}$$

3.2. Settlement of the Embankment after Construction

3.2.1. Settlement of an Embankment at Height z_I after Construction. The settlement of an embankment at height z_I after construction can be described as follows:

$$\Delta S(z_I)=\int_0^{z_I}\Delta\varepsilon(T_c,T_c+DT)dz. \tag{48}$$

Substituting equation (26) into equation (48) gives

$$\frac{\Delta S(z_I)E_H}{\gamma R}=a\left(1-e^{-DT}\right), \tag{49}$$

where the value of a is equal to equation (32).

At the top of the embankment,

$$I_1(T_c, T_c) = 0, \tag{50}$$

$$\frac{\Delta S(H)E_H}{\gamma R} = e^{-T_c}\left(1 - e^{-DT}\right)I_2(z, T_c). \tag{51}$$

If the height of the embankment varies linearly with time, with a slope of 1, then equations (49) and (51) will become

$$\frac{\Delta S(z_I)E_H}{\gamma R} = \left(z_I - e^{-z_I} + e^{-H}\right)\left(1 - e^{-DT}\right), \tag{52}$$

$$\frac{\Delta S(H)E_H}{\gamma R} = \left(H + e^{-H} - 1\right)\left(1 - e^{-DT}\right). \tag{53}$$

3.2.2. Settlement of a Finite Layer (z_I, z_{II}) after Construction. The strain of a finite layer (z_I, z_{II}) after construction is

$$\Delta\varepsilon = \frac{\Delta S(z_I, z_{II})}{\Delta z} = \frac{\Delta S(z_{II}) - \Delta S(z_I)}{\Delta z}, \tag{54}$$

The settlement of a finite layer (z_I, z_{II}) after construction is

$$\frac{\Delta S(z_I, z_{II})E_H}{\gamma R} = e^{-T_c}\left(1 - e^{-DT}\right)\Delta z\left[I_1(T_{II}, T_c) + b\right], \tag{55}$$

where

$$I_1(T_{II}, T_c) = \int_{T_{II}}^{T_c} e^T \frac{dz}{dT} dT = \sum_{i=II}^{i=N}\left(e^{T_i}\Delta z_i\right), \tag{56}$$

where the value of b is equal to equation (44).

3.3. Parameter Determination. The three parameters of the model are the elastic modulus E_H, the creep ratio R, and the time factor T_r.

If settlement is measured from different heights of the embankment, from equation (55), the time factor T_r is obtained from

$$\frac{\Delta S(T_c, T_2)}{\Delta S(T_c, T_1)} = \frac{1 - e^{-DT_2}}{1 - e^{-DT_1}} = \frac{1 - e^{-\Delta t_2/T_r}}{1 - e^{-\Delta t_1/T_r}}, \tag{57}$$

where Δt is the time increment after construction.

The solution of equation (57) with different time increments will permit an adjustment for T_r.

Substituting equation (55) into equation (42), the values of R from different layers are obtained:

$$R = \frac{Z_{II}}{e^{-T_c}\left[I_1(T_{II}, T_c) + b\right]\left[\left(\left(S(z_I, z_{II})\right)/\left(\Delta S(z_I, z_{II})\right)\right)\left(1 - e^{-DT}\right) + 1\right] - be^{-T_{II}}}. \tag{58}$$

Substituting the value of T_r and R into equation (41) gives

$$E_H = \frac{\gamma}{S(z_I, z_{II})}\left(Z_{II} - R\left[e^{-T_c}I_1(T_{II}, T_c) + b\left(e^{-T_c} - e^{-T_{II}}\right)\right]\right). \tag{59}$$

4. Practical Verification

For the Lanzhou–Yongjing highway, a section from 24 + 160 km to 25 + 838 km was completed with a high-fill subgrade. The settlement meters were set up from 24 + 400 km to 24 + 405 km, which was semifilling and semiexcavating subgrades (Figure 5(a)). On the right side of the subgrade, a steep slope was there. However, flood drainage was on the left side of the subgrade. The materials excavated from the slope were used to fill the subgrade. The maximum fill height of this section was 18.3 m. From 0 to 15 m height, the subgrade was filled with loess. From 15–16.1 m height, it was filled with a sandy pebble. From 16.1–18.3 m height, it was filled with gravel. The physical and mechanical properties of the subsoils are shown in Table 1. Single-point settlement meters were adopted to monitor the long-term settlement of the subgrade [29]. It can be seen that for both the road shoulder and driveway, 6 layers of settlement meters were embedded. The layout of settlement meters is shown in Figure 5, which were 3 m, 6 m, 9 m, 12 m, 15 m, and 18.3 m. And the embedment depth is reflected in Figure 5(b). Almost two-year settlement data are obtained from the embankment after construction. And the field-measurement settlement data during construction is obtained from [28], which monitored the settlement of each layer of the filling during the construction, and the relationship between filling height and settlement of the filling during construction is represented in Figure 6. And from the monitored data during construction in Figure 6, firstly, the value of T_r is obtained from equation (57), secondly, substituting the value of T_r and all the monitored parameters into equation (58) to calculate the value of R, thirdly, the values of T_r and R are substituted into equation (59) to get the value of E_H, and finally, the creep settlement of every layer of the embankment is calculated from equations (42) and (55), respectively, which are presented in Figures 7 and 8. From the field-measured data, the T_r, R, and E_H parameters for every layer were established as indicated in Table 2.

Settlement values during construction from field measurement and settlement values calculated from equation (31) are presented in Figure 6, which is basically consistent with the experimental finding [30].

The measured and calculated settlements after construction obtained with equation (49) are presented in Figure 7.

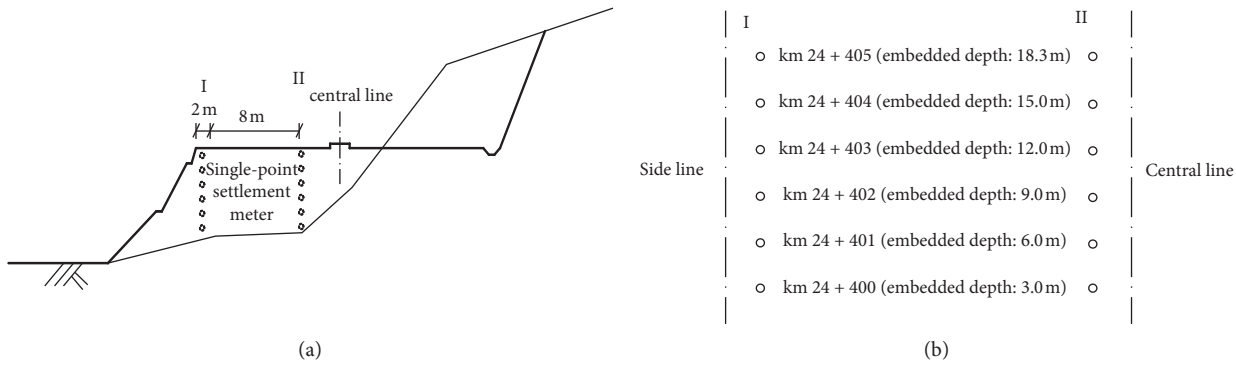

Figure 5: Single-point settlement meters. (a) Layout profile. (b) Planar graph (reproduced from Jia et al. [28] (under the Creative Commons Attribution License/public domain)).

Table 1: Physical and mechanical parameters of subsoil (reproduced from Jia et al. [28] (under the Creative Commons Attribution License/public domain)).

Soil type	Thickness (m)	Moisture content (%)	Gravity ($kN \cdot m^3$)	Void ratio	Compression coefficient (MPa^{-1})	Compression modulus (MPa)	Bearing capacity eigenvalues (kPa)
Loess	10.4	8.5	14.1	0.96	0.21	6.2	150
Loess	4.8	16.5	14.9	0.89	0.23	7.6	180
Pebble	3.3	21	24.8	1.15	—	—	400
Mudstone	—	—	25.3	—	—	—	600

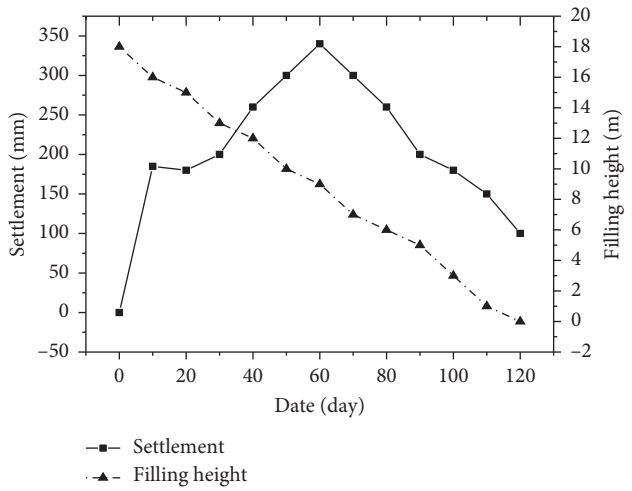

Figure 6: Relationship between filling height and settlement of the filling during construction.

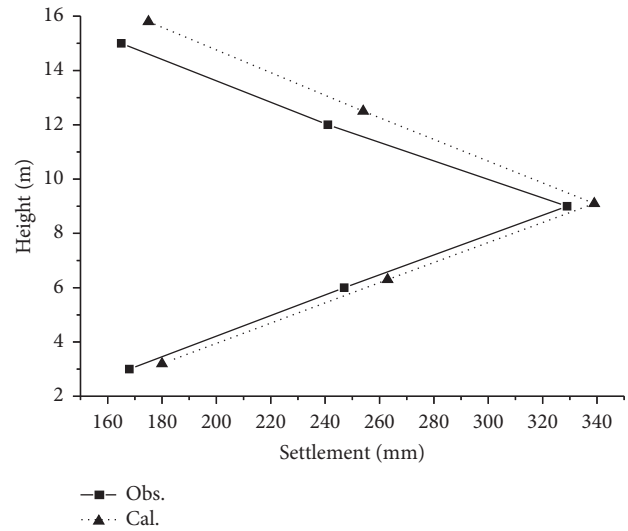

Figure 7: Comparison between observed and calculated settlements during construction.

The agreement between the measured and calculated settlements is excellent, although the measured settlement values are more irregular because this area is in a soil region that is seasonally frozen, and during the winter, soil freezing leads to the ground heave [31, 32].

5. Conclusions

To describe the time-dependent behavior of clay inside a high-filled embankment, the viscoelastic model of Poynting–Thomson was applied in this study in order to calculate the creep settlement of high-filled embankments. And the stress history is reflected by the hereditary integral. One-dimensional compression was assumed in this investigation. The settlement values at a point and of a finite layer during construction and after construction are obtained. The three parameters of this model, T_r, R, and E_H, can be adjusted for the in situ monitoring data from every layer. By comparison of calculated results obtained by the proposed method with the field monitoring data, it was concluded that the proposed method can give a precise prediction of the creep settlement of high-filled embankments. In the future work, the other viscoelastic models which can better reflect the time-dependent creep behavior of

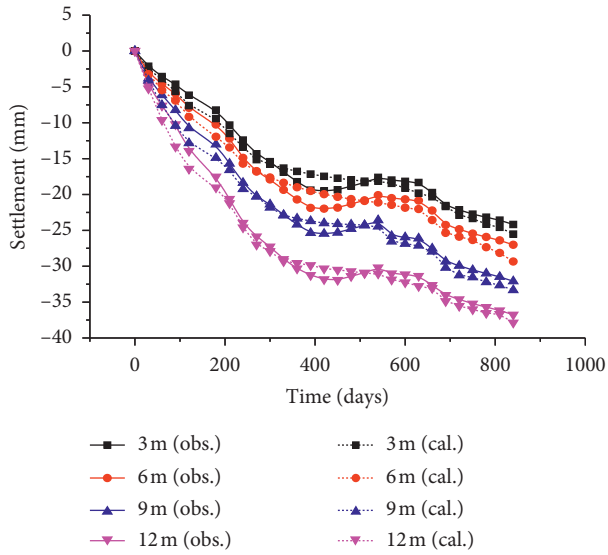

Figure 8: Comparison between observed and calculated settlements after construction.

Table 2: Creep parameters of every layer.

Fill stratum	T_r	E_H	R
3 m~6 m	172.8312	0.0373	0.0072
6 m~9 m	172.8342	0.0378	0.0103
9 m~12 m	172.8387	0.0370	0.0174
12 m~15 m	172.8377	0.0368	0.0385

soils will apply to amplify understanding of settlement behavior in more complex soil conditions.

Data Availability

The data used to support the findings of this study are included within the article.

Conflicts of Interest

The authors declare that there are no conflicts of interest.

Acknowledgments

This work was financially supported by the National Natural Science Foundation of China (Grant no. 51568044).

References

[1] J. Liu, W. Liu, P. Liu, C. Yang, Q. Xie, and Y. Liu, "Preliminary research on the theory and application of unsaturated red-layers embankment settlement based on rheology and consolidation theory," *Environmental Earth Sciences*, vol. 75, no. 6, p. 503, 2016.

[2] Y. Q. Tang, X. Ren, B. Chen, S. Song, J. X. Wang, and P. Yang, "Study on land subsidence under different plot ratios through centrifuge model test in soft-soil territory," *Environmental Earth Sciences*, vol. 66, no. 7, pp. 1809–1816, 2012.

[3] S. Wang, J. Qi, and F. Liu, "Study on the reasonable height of embankment in Qinghai-Tibet highway," *Geotechnical and Geological Engineering*, vol. 34, no. 1, pp. 1–14, 2016.

[4] H. Peng, W. Ma, Y.-H. Mu, and L. Jin, "Impact of permafrost degradation on embankment deformation of Qinghai-Tibet highway in permafrost regions," *Journal of Central South University*, vol. 22, no. 3, pp. 1079–1086, 2015.

[5] J. Wei, Z. Song, Y. Bai, J. Liu, D. Kanungo, and S. Sun, "Field test and numerical simulation for coordinated deformation of new subgrade and old embankment adjacent to river," *Applied Sciences*, vol. 8, no. 12, p. 2334, 2018.

[6] R. Nazir, N. Sukor, H. Niroumand, and K. A. Kassim, "Performance of soil instrumentation on settlement prediction," *Soil Mechanics and Foundation Engineering*, vol. 50, no. 2, pp. 61–64, 2013.

[7] H. Wang, W.-Z. Chen, Q.-B. Wang, and P.-Q. Zheng, "Rheological properties of surrounding rock in deep hard rock tunnels and its reasonable support form," *Journal of Central South University*, vol. 23, no. 4, pp. 898–905, 2016.

[8] T. S. Tan, T. Inoue, and S. L. Lee, "Hyperbolic method for consolidation analysis," *Journal of Geotechnical Engineering*, vol. 117, no. 11, pp. 1723–1737, 1991.

[9] Y. Xu and Z. Xu, "A new method to predict the settlement of embankment," *Journal of Hohai University*, vol. 28, no. 5, pp. 111–113, 2000, in Chinese.

[10] A. S. Al-Homoud and N. Tanash, "Monitoring and analysis of settlement and stability of an embankment dam constructed in stages on soft ground," *Bulletin of Engineering Geology and the Environment*, vol. 59, no. 4, pp. 0259–0284, 2001.

[11] D. T. Bergado, P. M. Daria, C. L. Sampaco, and M. C. Alfaro, "Prediction of embankment settlement by in-situ tests," *Geotechnical Testing Journal*, vol. 14, no. 4, pp. 425–439, 1991.

[12] L. Bjerrum, "Engineering geology of Norwegian normally-consolidated marine clays as related to settlements of buildings," *Géotechnique*, vol. 17, no. 2, pp. 83–118, 1967.

[13] Y. P. Yao, L. M. Kong, A. N. Zhou, and J. H. Yin, "Time-dependent unified hardening model: three-dimensional elastoviscoplastic constitutive model for clays," *Journal of Engineering Mechanics*, vol. 141, no. 6, article 04014162, 2014.

[14] K. Hashiguchi, "Subloading surface model in unconventional plasticity," *International Journal of Solids and Structures*, vol. 25, no. 8, pp. 917–945, 1989.

[15] A. Asaoka, M. Nakano, and T. Noda, "Elasto-plastic behavior of structured over consolidated soils," *Journal of Applied Mechanics*, vol. 3, pp. 335–342, 2000.

[16] Z. C. Wang, D. M. Kuang, T. Zhao, Y. S. Luo, and W. G. Wang, "Research on a calculation method and three-dimensional simulation of a high-filled embankment rheological settlement," in *Proceedings of the Geo-China 2016*, pp. 201–209, Shandong, China, July 2016.

[17] N. Loganathan, A. S. Balasubramaniam, and D. T. Bergado, "Deformation analysis of embankments," *Journal of Geotechnical Engineering*, vol. 119, no. 8, pp. 1185–1206, 1993.

[18] Y. Li, Y. Xie, and B. Liu, "Application of modified secant modulus method in settlement calculation," *Journal of Highway and Transportation Research and Development (English Edition)*, vol. 4, no. 1, pp. 35–39, 2009.

[19] Z. C. Wang, Y. S. Luo, and S. H. Tang, "Mechanism and calculation method of rheological settlement of high-filled embankment," *Journal of Central South University of Technology*, vol. 15, no. 1, pp. 381–385, 2008.

[20] D. D. Khaidapova, V. V. Klyueva, E. B. Skvortsova, and K. N. Abrosimov, "Rheological properties and tomographically determined pore space of undisturbed samples of

typical chernozems and soddy-podzolic soils," *Eurasian Soil Science*, vol. 51, no. 10, pp. 1191–1199, 2018.

[21] B.-N. Ma, X.-Y. Xie, and K.-F. Liu, "Rheological catastrophic model for soft clays," *Journal of Central South University*, vol. 19, no. 8, pp. 2316–2322, 2012.

[22] Z. L. Wang, J. Z. Huang, and Y. C. Li, "Study on application of Asaoka's method to settlement prediction," *Yantu Lixue(Rock and Soil Mechanics)*, vol. 27, no. 11, pp. 2025–2028, 2006.

[23] A. Morro, "Modelling of viscoelastic materials and creep behaviour," *Meccanica*, vol. 52, no. 13, pp. 3015–3021, 2017.

[24] J. L. Justo and P. Durand, "Settlement-time behaviour of granular embankments," *International Journal for Numerical and Analytical Methods in Geomechanics*, vol. 24, no. 3, pp. 281–303, 2000.

[25] R.-F. Fung, J.-S. Huang, and Y.-C. Chen, "The transient amplitude of the viscoelastic travelling string: an integral constitutive law," *Journal of Sound and Vibration*, vol. 201, no. 2, pp. 153–167, 1997.

[26] Y. A. Rossikhin and M. V. Shitikova, "Applications of fractional calculus to dynamic problems of linear and nonlinear hereditary mechanics of solids," *Applied Mechanics Reviews*, vol. 50, no. 1, pp. 15–67, 1997.

[27] A. Shukla and Y. M. Joshi, "Boltzmann superposition principle for a time-dependent soft material: assessment under creep flow field," *Rheologica Acta*, vol. 56, no. 11, pp. 927–940, 2017.

[28] L. Jia, J. Guo, and K. Yao, "In situ monitoring of the long-term settlement of high-fill subgrade," *Advances in Civil Engineering*, vol. 2018, Article ID 1347547, 9 pages, 2018.

[29] M. M. Ge, N. Li, and W. Zhang, "Settlement behavior and inverse prediction of post-construction settlement of high filled loess embankment," *Chinese Journal of Rock Mechanics and Engineering*, vol. 36, no. 3, pp. 745–753, 2017.

[30] H. J. Jing, C. S. Hu, and B. G. Wang, "Study on settlement and deformation laws of high loess-fill embankment," *Yanshilixue Yu Gongcheng Xuebao/Chinese Journal of Rock Mechanics and Engineering*, vol. 24, pp. 5845–5850, 2005.

[31] H. Hettiarachchi, "Settlement behavior of bioreactor landfills in North America," in *Proceedings of the Geo Congress 2012: State of the Art and Practice in Geotechnical Engineering*, pp. 4222–4231, Oakland, CA, USA, March 2012.

[32] Z. Li, W. Ye, M. Marence, and J. Bricker, "Unsteady seepage behavior of an earthfill dam during drought-flood cycles," *Geosciences*, vol. 9, no. 1, p. 17, 2019.